2018

Development and Validation of a Semi-Empirical Model for Two-Phase Heat Transfer from Arrays of Impinging Jets

C. Mira-Hernández
Purdue University

M. D. Clark
Purdue University

J. A. Weibel
Purdue University, jaweibel@purdue.edu

S V. Garimella
Purdue University, sureshg@purdue.edu

Mira-Hernández, C.; Clark, M. D.; Weibel, J. A.; and Garimella, S V., "Development and Validation of a Semi-Empirical Model for Two-Phase Heat Transfer from Arrays of Impinging Jets" (2018). *CTRC Research Publications.* Paper 326.
http://dx.doi.org/https://doi.org/10.1016/j.ijheatmasstransfer.2018.03.047

Development and Validation of a Semi-Empirical Model for Two-Phase Heat Transfer from Arrays of Impinging Jets[1]

Carolina Mira-Hernández[*], Matthew D. Clark[*], Justin A. Weibel, Suresh V. Garimella[2]

School of Mechanical Engineering

Purdue University, 585 Purdue Mall, West Lafayette, IN 47907 USA

Abstract

Two-phase jet impingement is a compact cooling technology that provides high-heat-flux dissipation at manageable pressure drop, with applications in cooling power electronics and server modules. The extensive set of geometrical parameters and operating conditions that determine the heat transfer behavior of jet impingement systems provide an attractive level of design flexibility. In the present study, a semi-empirical approach is developed to predict heat transfer from arrays of jets of liquid that undergoes phase change upon impingement. In the modeling approach developed, the jet array is divided into unit cells centered on each orifice that are assumed to behave identically. Based on prior experimental observations, the impingement surface in each unit cell is divided into two distinct regions: a single-phase heat transfer region directly under the jet, and a surrounding boiling heat transfer region along the periphery. Single-phase convection and boiling heat transfer correlations available in the literature are used to estimate the heat transfer coefficient distribution in each region, and the mean surface temperature of the unit cell is estimated via area-averaging. An analysis is performed to show that the model outputs are sensitive to the heat transfer coefficient correlations used as inputs, with the choice depending on the heat flux input and the expected operating regime. Experiments are performed to validate the area-averaged thermal performance predictions. The model results are also compared against experimental data in the literature. The semi-empirical modeling approach developed in this work successfully represents the different heat transfer modes and transitions that occur during two-phase jet impingement. The location of transition to boiling predicted by the model is consistent with prior experimental observations of an inward-creeping boiling front with increasing heat flux. The predicted temperature difference between the surface and the jet inlet across all experimental comparisons has a mean absolute percentage error of 3.88%. The proposed modeling approach is demonstrated to be a practical tool in the development of two-phase jet array impingement devices, allowing for parametric exploration across the expansive design space.

Keywords

Electronics cooling, jet impingement, boiling, two-phase flow, prediction, model

---

[1] Submitted for possible publication in *International Journal of Heat and Mass Transfer*, 2017.

[2] Corresponding author, Tel.: +1 765 494 5621. E-mail address: sureshg@purdue.edu.

[*] These authors contributed equally to this work

Nomenclature

A_c	jet unit cell area (s^2)
A_f	ratio of orifice area to cell area ($\pi/(4(s/d)^2)$)
C	constants in heat transfer profile
c_p	liquid specific heat
d	orifice diameter
H	orifice-to-target spacing
h	local convective heat transfer coefficient
$\bar{h}$	area-averaged heat transfer coefficient
h_0	stagnation-point heat transfer coefficient
k	liquid thermal conductivity
l	orifice plate thickness
M	fluid molecular mass
$\dot{m}$	mass flow rate
N	number of jets in the array
Nu	local Nusselt number (hd / k)
$\overline{\mathrm{Nu}}$	area-averaged Nusselt number ($\bar{h}d / k$)
Nu_0	stagnation Nusselt number ($h_0 d / k$)
p_c	fluid critical pressure
p_{op}	operating pressure
Pr	liquid Prandtl number ($c_p \mu / k$)
q''	heat flux
r	radial distance from stagnation point
r_{eq}	equivalent radius of jet unit cell ($s / \sqrt{\pi}$)
R_p	peak roughness
Re	Reynolds number ($\rho v_j d / \mu$)
s	jet-to-jet spacing and square unit cell dimension
T	temperature
ΔT_{sub}	degree of subcooling (T_{sat} - T_j)
v	velocity

Greek symbols

μ	liquid dynamic viscosity
ρ	liquid density
σ	heat transfer profile width parameter

Subscript

f	evaluated at film temperature
j	jet inlet condition
nb	nucleate boiling region
ref	reference heat transfer value for single-phase jet impingement
s	surface condition
sat	saturated condition
sp	single-phase heat transfer region

1 Introduction

Two-phase jet impingement is an attractive approach for cooling densely packed electronics systems due to the integration of highly effective heat transport mechanisms into a compact and flexible design. The heat transfer behavior of an impinging jet array is dependent on many design parameters, such as the orifice dimensions, array size and distribution, orifice-to-target spacing, and operating/boundary conditions, as illustrated in Figure 1. Prediction of the heat transfer performance when the jets undergo phase change is particularly challenging due to the coupled phase-change phenomena and flow dynamics. On the other hand, exhaustive parametric evaluation via experimentation is infeasible.

During two-phase jet impingement, both single-phase convection and boiling occur concurrently at different regions of the heat transfer surface. On a smooth, flat surface, nucleate boiling initiates at the periphery of the wall jet as the heat flux is increased, and creeps inwards toward the stagnation region directly under the jet orifice [1–3]. In a study that used infrared thermography to measure the temperature of a thin-film heater cooled by jet array impingement, Rau and Garimella [1] observed a stable boiling front, beginning furthest away from the jet centers and moving inward with increasing heat flux. At the highest heat fluxes tested, the boiling front reached the jet centers ($r_{nb} / d = 0$), such that boiling occurred across the entire surface. The behavior of the boiling front was also investigated by Dukle and Hollingsworth [4–5] using liquid crystal thermography in a submerged unconfined liquid jet. They found that the boiling front was marked by the location at which the level of wall superheat was sufficient to cause nucleation. Because the local wall superheat in the single-phase region is controlled by the local convective transport, a correlation between the location of the boiling front and the convection coefficient profile was identified [4–5]. Orifice-to-target spacing, jet-to-jet spacing, jet diameter, and jet velocity determine the shape of this local convection coefficient profile [6–8].

In submerged jet impingement, the local single-phase heat transfer coefficient achieves a maximum value near the stagnation point under the jet orifice and decreases radially outward in a monotonic fashion as the wall jet boundary layer grows in thickness [1,5,6,9,10]. In some cases, a secondary peak in the local convection coefficient has been observed to occur at a short radial distance from the stagnation region [5], and is associated with transition to turbulence in the wall jet; in confined jet impingement, this transition is also associated with reattachment of the recirculating flow pattern created by the confinement gap [11–12]. This secondary peak is more significant at higher jet Reynolds numbers and smaller orifice-to-target spacings [7,11]. In jet arrays with significant jet-to-jet interactions, the secondary peak is less pronounced than for a single jet [6].

Correlations that predict the local and average convection coefficient during single-phase jet impingement heat transfer have been developed [13–17]. Chang *et al.* [13] correlated both local and average single-phase heat transfer data for a single jet and compared these correlations with average heat

transfer data from jet arrays. Using fluids with Prandtl numbers ranging from 0.7 to 25.2, Li and Garimella [15] developed correlations for both area-averaged convection coefficients and stagnation-point convection coefficients that took into account fluid-property dependence. Martin [16] developed such single-phase correlations for single round and slot nozzles, as well as for arrays of nozzles. Campbell *et al.* [17] performed experiments over a relatively wide range of Reynolds numbers (141 - 6670), small jet diameters (0.377 mm – 1.01 mm), and large numbers of jets (16 – 324) and developed a correlation for area-averaged convection coefficients. For two-phase jet impingement, Chang *et al.* [10] proposed a correlation based on superposition of nucleate boiling and single-phase convective heat transfer mechanisms. Buchanan and Shedd [18] also proposed a superposition-based correlation; one mode of heat transfer is suppressed when the other is dominant.

The current work develops and validates a semi-empirical model to predict area-averaged two-phase heat transfer from arrays of impinging jets. The model considers confined and submerged liquid jet arrays impinging on a smooth, flat surface generating a uniform heat flux. The model separately treats the single-phase and boiling regions, and thereby is uniquely able to provide performance predictions across the single-phase, partial boiling, and fully boiling heat transfer regimes that have been observed experimentally. Correlations from the literature are used to predict the single- and two-phase heat transfer coefficients in sub-regions of a unit cell under each jet. An analysis is performed to assess sensitivity of the model outputs to changes in key input parameters. Experiments are performed for different orifice-to-target spacings and array geometries to validate the model. The model predictions are also compared against experimental data available in the literature.

2 Model description

The jet impingement system being modeled is illustrated in Figure 2. Liquid jets are formed when subcooled liquid passes through an orifice plate with a square array of circular orifices. The flow through all the orifices is assumed to have the same, constant inlet temperature and to be equally distributed among the orifices, yielding jets of the same velocity. The jets issue into a gap filled with the same fluid, leading to a submerged jet impingement situation. The jets impinge on a flat surface that is being heated at a uniform flux. As heat is removed from the surface and the temperature of the fluid increases, boiling may occur either in selected regions or over the entire surface. After impingement, the spent fluid is forced outwards through the confinement gap bounded on the top and bottom by the orifice plate and the impingement surface, respectively. The resultant average temperature of the surface depends on a set of geometrical parameters, operating conditions, and fluid properties. The geometrical parameters accounted for in the model include the jet diameter, orifice-to-target spacing and jet-to-jet spacing; the operating conditions include the fluid flow rate, operating pressure, inlet subcooling, and surface heat flux.

2.1 Unit-cell-based modeling approach

The jet array is divided into unit cells, as shown in Figure 2(a), which are assumed to have identical, spatially periodic heat transfer behavior. Inside each unit cell, two distinct regions are identified at each heat flux, namely, a region undergoing single-phase convective heat transfer and another undergoing nucleate boiling heat transfer. Figure 2(b) shows this division inside each unit cell schematically. These regions are in concordance with the experimental observation of boiling starting at the periphery of the wall jet (in the regions between neighboring jets), and creeping inwards towards the stagnation region as the heat flux increases [1].

As shown in Figure 2(c), it is assumed that heat transfer in the single-phase region is identical to that for a reference case in which only single-phase jet-impingement heat transfer occurs across the entire unit cell. In the boiling region, on the other hand, a uniform nucleate pool boiling coefficient is assumed, similar to the behavior reported by Rau and Garimella [1]. The area-averaged surface temperature inside the jet unit cell is then found as:

$$\overline{T_s} = \frac{q''}{A_c}\left(\int_{A_{sp}} \frac{1}{h_{ref}\left(r\right)} dA + \frac{A_{nb}}{h_{nb}} \right) + T_j \tag{1}$$

To delineate the regions, the model assumes that nucleate boiling occurs in those regions of the unit cell where the heat transfer coefficient due to nucleate boiling exceeds that due to single-phase convection. Hence, the location of the boiling front is defined at the intersection of the single-phase heat transfer profile and the horizontal line representing a constant nucleate pool boiling heat transfer coefficient, as shown in Figure 2(c). The single-phase heat transfer coefficient is assumed to monotonically decrease from the stagnation point, and a unique intersection point is found at the radial coordinate where:

$$h_{ref}\left(r\right)\Big|_{r=r_{nb}} = h_{nb} \tag{2}$$

A nucleate pool boiling correlation appropriate for the surface-fluid combination can be used to estimate the boiling heat transfer coefficient. The assumed functional form of the single-phase heat transfer coefficient profile for jet impingement is described in Section 2.2, and requires as inputs empirical correlations for the area-averaged and the stagnation heat transfer coefficient.

Details regarding the computation of the area of the boiling region for a square unit cell are presented in the appendix. The area of the single-phase region is simply found as:

$$A_{sp} = A_c - A_{nb} \tag{3}$$

To facilitate the evaluation of the area-integral in the single-phase region in Eq. (1), this region is approximated as a circular area of radius:

$$r_{sp} = A_{sp} \Big/ \sqrt{\pi} \tag{4}$$

The average surface temperature is then computed as:

$$\overline{T_s} \approx \frac{q''}{A_c}\left(2\pi \int_0^{r_{sp}} \frac{1}{h_{ref}\left(r\right)} dr + \frac{A_{nb}}{h_{nb}} \right) + T_j \tag{5}$$

2.2 Single-phase heat transfer coefficient profile

The single-phase heat transfer profile used in the model is inspired by prior experimental observations during jet impingement of a bell-shaped local heat transfer coefficient distribution with a maximum value at the stagnation point and a monotonic decrease in the outward radial direction [13]. The following function is proposed for the single-phase heat transfer coefficient.

$$\frac{1}{h_{ref}\left(r\right)} = \frac{\left(T_{s,ref}\left(r\right) - T_j\right)}{q''} = C_1 - C_2 \exp\left(\frac{-r^2}{2\sigma^2} \right) \tag{6}$$

The function is expressed as the inverse of the local heat transfer coefficient in order to facilitate the estimation of the area-averaged surface temperature by Eq. (1). The profile does not account for the possible existence of a secondary peak in the single-phase heat transfer coefficient distribution. Such a secondary peak has been observed in cases with small orifice-to-target spacings, large jet-to-jet spacings, and high Reynolds numbers [7].

The width parameter of the single-phase heat transfer profile, σ, is set as 1, which implies that the inflection point of the profile occurs near the transition from impingement to wall jet behavior at r/d = 1. Also, the profile is constrained to comply with the empirical values for the stagnation heat transfer coefficient and the area-averaged heat transfer coefficient:

$$h_{ref}\left(r\right)\Big|_{r=0} = h_{0,ref} \tag{7}$$

$$\frac{1}{A_c} \int_{A_c} \frac{1}{h_{ref}\left(r\right)} dA = \frac{1}{\overline{h_{ref}}} \tag{8}$$

Correlations appropriate to the specific geometrical parameters and operating conditions can be used for the area-averaged and the stagnation heat transfer coefficient. For the single-phase heat transfer correlations, fluid properties are evaluated at a film temperature, taken as the mean value of the jet inlet temperature and reference average surface temperature that would be achieved by single-phase jet impingement in the absence of boiling.

The square unit cell is approximated to a circular area of radius:

$$r_{eq} = s \Big/ \sqrt{\pi} \tag{9}$$

Eq. (7) and Eq. (8) are combined to determine the constants in the single-phase heat transfer profile, C_1 and C_2:

$$C_1 = \frac{\frac{1}{\bar{h}_{ref}} - \frac{1}{h_{0,ref}}\left\{\frac{2\sigma^2}{r_{eq}^2}\left[1-\exp\left(\frac{-r_{eq}^2}{2\sigma^2}\right)\right]\right\}}{1-\frac{2\sigma^2}{r_{eq}^2}\left[1-\exp\left(\frac{-r_{eq}^2}{2\sigma^2}\right)\right]} \tag{10}$$

$$C_2 = \frac{\frac{1}{\bar{h}_{ref}} - \frac{1}{h_{0,ref}}}{1-\frac{2\sigma^2}{r_{eq}^2}\left[1-\exp\left(\frac{-r_{eq}^2}{2\sigma^2}\right)\right]} \tag{11}$$

3 Experimental methods

Experiments are conducted to provide data for validation of the modeling approach, namely, the prediction of the area-averaged surface temperature and the different heat transfer modes and transitions that occur during two-phase jet impingement.

3.1 Flow loop

The custom-developed two-phase jet impingement facility used in the experiments is described in detail in Ref. [19] and is shown schematically in Figure 3. The dielectric liquid HFE-7100 [20] is circulated through the loop by a magnetically coupled gear pump, and the flow rate is coarsely set by tuning the rotation speed of the pump. Fine adjustments to the flow rate are then made using metering valves in the bypass loop line and at the test section inlet. Mass flow rate is measured by a Coriolis flow meter (CMFS015, Emerson) with +/- 0.1% accuracy. Subcooling at the jet inlet is maintained at 8 °C by adjusting the voltage supplied to a 1.2 kW inline preheater. For degassing purposes, the reservoir is equipped with a 1 kW immersion heater and two Graham reflux condensers connected to a chiller. Fluid exiting the reservoir is cooled before entering the pump by a copper-finned liquid-to-air heat exchanger equipped with a voltage-regulated fan; this prevents cavitation in the pump and provides greater control over the jet inlet subcooling temperature.

3.2 Test section

The test section, shown in Figure 4, was originally developed in Ref. [19], but the heater assembly was modified for the current study to ensure that the heated surface is completely covered by the jet array, so as to achieve spatially periodic unit cells. The specific modifications include a smaller heater surface area and new orifice plates with the jet arrays spanning over a larger area. The walls of the test section are

constructed of polyether ether ketone (PEEK) for thermal insulation and include polycarbonate front and back walls for visualization. Fluid enters through the top of the test section into the cylindrical plenum, where it passes through two screens and a honeycomb to condition the flow. Inlet pressure and temperature are respectively measured by a pressure tap and a T-type thermocouple placed just upstream of the jet array. The jet array is formed by an interchangeable orifice plate sealed by an O-ring to the bottom of the plenum. Two different array geometries are studied for the current experiments, namely, a 3×3 square array of 2 mm-diameter round jets and a 5×5 square array of 1.2 mm-diameter round jets. In both cases, the orifice aspect ratio l/d is chosen to be 2 and the nondimensional jet-to-jet spacing s/d is 3.33. Both arrays have the same total open orifice area, resulting in equal jet velocities for a given flow rate. The orifice-to-target spacing (H/d) is precisely set by resting the orifice plate on three spacer pins inserted into the bottom of the test section. An O-ring creates a seal between the plenum and the PEEK ceiling of the test section, allowing the plenum to translate vertically so that its position can be adjusted to provide the required confinement height.

Jets issue from the orifice plate into submerged conditions and spent fluid exits through an outlet port at the top of the test section. Pressure at the outlet of the jets is measured with a pressure tap (Gems 2200BG3F002A3UA) in the bottom of the test section. Insertion of a T-type thermocouple through the side wall of the test section allows measurement of the fluid bath temperature.

The jets impinge on a 20 mm × 20 mm square heated surface, which is aligned such that it is completely covered by an integer number of square unit cells with a side length equal to the jet-to-jet spacing (3.33 jet diameters). The test surface is heated by means of twelve 100 W cartridge heaters inserted into the bottom of an oxygen-free copper block. The copper block is equipped with three thermocouple rakes located along the centerline and along two opposing sidewalls of the block, which allow for calculation of the area-averaged surface temperature from extrapolated surface values obtained for the three rakes. The centerline rake consists of four T-type thermocouples inserted at 2.54 mm intervals in the vertical direction. The near-sidewall rakes consist of two T-type thermocouples each, spaced by 7.62 mm vertically. Fiberglass insulation is packed into the cavities between the heater block and the surrounding PEEK carrier; the heater block is supported from below by a ceramic block to provide further insulation. The smooth top surface of the heater is mounted flush with the bottom of the test section and a small bead of sealant (Q3-6611, Dow Corning) is carefully applied into a 1 mm chamfer cut into the tightly fitting 4 mm thick PEEK plate surrounding the edges of the test surface. By applying the sealant into a recessed chamfer, the bead can be made smooth and flush with the upper edges of the heater block and the surrounding PEEK plate, while maintaining proper adhesion to the copper side walls.

3.3 Experimental procedure

Prior to each test run, the HFE-7100 in the flow loop is degassed by circulating it at a flow rate of 650 ml/min while using the immersion heater and the inline heater to boil the fluid. Noncondensable gases are allowed to vent to the atmosphere through the two Graham reflux condensers on the reservoir. This initial degassing procedure is carried out for 2 h. During experimentation, the facility is run in an open-loop configuration, using the immersion heater to maintain the fluid in the reservoir at the saturation temperature corresponding to the atmospheric pressure (101.3 kPa), while continuing to vent noncondensable gases to the atmosphere. This ensures that the HFE-7100 remains degassed throughout the experiment.

The HFE-7100 flow rate desired for testing (1300 ml/min in all cases presented here) is then set, and the power input to the inline heater is adjusted to maintain an inlet subcooling of 8 °C, relative to the saturation temperature calculated according to the outlet pressure. Power input to the heater block is incremented in steps of 8 W, and 2 min of steady-state data are collected at each step. The system is considered to be at a steady state when a surface temperature change of less than 1 °C/h is measured. Data are recorded at a frequency of 0.5 Hz, capturing 60 steady-state measurements per step.

Experiments were performed at nondimensional orifice-to-target distances (H/d) of 4, 1, and 0.5 for the 3×3 array, corresponding to actual confinement heights (H) of 8 mm, 2 mm, and 1 mm, respectively. Nondimensional orifice-to-target distances of 4 and 1 were tested for the 5×5 array, corresponding to actual confinement heights of 4.8 mm and 1.2 mm, respectively. All experiments were carried through to a critical heat flux condition, as indicated by a rapid surface temperature rise upon incrementing power to the heater block. The final reported data point corresponds to the steady-state data recorded prior to the sudden temperature rise. A summary of experimental conditions is provided in Table 1.

3.4 Data reduction

The area-averaged surface temperature of the copper heater is extrapolated from the temperature gradient inside the block measured by the thermocouple rakes, assuming one-dimensional conduction. Thermocouple measurement uncertainties are estimated to be ±0.3 °C, such that the average surface temperature extrapolation resulted in an uncertainty from ±0.4 °C at a low heat flux to ±0.6 °C at the maximum heat flux of 49 W/cm^2. Heat loss from the block is estimated by a numerical heat loss model, following the procedure in Ref. [19], and is subtracted from the electrical power supplied to the heater for calculation of heat flux to the fluid. Uncertainty in heat flux was estimated to be less than 2% based on a 95% confidence interval. All uncertainties are calculated as described in Ref. [19].

4 Predicted behavior and model sensitivity

To demonstrate the heat transfer behavior predicted by the model as a function of heat flux, a baseline array geometry is chosen that matches one of the current experimental cases. This geometry consists of a 3×3 array of 2 mm-diameter round orifices with an aspect ratio (*l/d*) of 2, an orifice-to-target spacing (*H/d*) of 4, and jet-to-jet spacing (*s/d*) of 3.33. As in the current experiments, the working fluid is HFE-7100 with an inlet subcooling of 8 °C (T_{in} = 51 °C), operating pressure of 101.3 kPa, and jet velocities of 1 and 4 m/s. For this baseline geometry and operating conditions, the same correlations are used as for the model validation in Section 5.1 as presented in Table 2. At this baseline, the sensitivity of the model predictions to changes in key model input variables is also assessed by calculating the bounds of the model outputs for a $\pm 15\%$ change from the baseline case in each of the model input variables considered. The four model input variables studied are the average single-phase Nusselt number ($\overline{\mathrm{Nu}}_{ref}$), the single-phase stagnation Nusselt number ($\mathrm{Nu}_{0,ref}$), the single-phase width parameter (σ), and the nucleate boiling heat transfer coefficient (h_{nb}). The variables allow an assessment of the sensitivity of the model to the primary empirical inputs in each heat transfer regime, as well as a confirmation that the assumed functional form of the single-phase heat transfer profile does not significantly influence the predictions.

In Figure 5(a), boiling curves show the predicted surface superheat (defined as the difference between the area-averaged surface temperature and the saturation temperature of the fluid ($\overline{T_s} - T_{sat}$)) as a function of the surface heat flux. The bounding envelopes in Figure 5(a) correspond to the deviation of predicted superheat from the baseline prediction, represented by a solid black line, for changes in two empirical inputs. The blue shaded envelope corresponds to a ±15% change in the average single-phase Nusselt number ($\overline{\mathrm{Nu}}_{ref}$), while the gray shaded envelope corresponds to a ±15% change in the nucleate pool boiling heat transfer coefficient (h_{nb}). In Figure 5(b), the predicted normalized heat transfer coefficient distributions (h/h_0) are plotted within a unit cell for three different heat fluxes at the higher jet velocity of 4 m/s; these predictions correspond to the baseline values as indicated by the matching symbols on the boiling curves in Figure 5(a).

While prediction of the *local* heat transfer coefficient distributions is not the objective of the model, Figure 5(b) is useful to illustrate the heat transfer behavior predicted by the model as a function of heat flux. The three heat fluxes shown in Figure 5(b) are chosen to represent the three main regimes in two-phase jet impingement: the single-phase regime, the partial boiling regime, and the fully boiling regime. During purely single-phase operation at 12 W/m^2, the model predicts a local heat transfer coefficient distribution strictly according to the proposed single-phase profile. During the partial boiling regime, at 18 W/m^2, boiling is predicted to occur over an outer region within each jet unit cell, and a transition can

be seen from the bell-shaped single-phase profile to the constant nucleate pool boiling heat transfer coefficient. During the fully boiling regime, at 25 W/m^2, the model predicts boiling to occur across the entire surface.

At low heat fluxes, the area-averaged behavior in Figure 5(a) follows the single-phase prediction, which has a constant area-averaged heat transfer coefficient with increasing heat flux, seen as a linear slope in the boiling curves. Once boiling begins in the partial boiling regime, the area-averaged heat transfer coefficient increases due to inclusion of the nucleate boiling heat transfer coefficient (h_{nb}) in the boiling regions on the surface. The curves in Figure 5(a) corresponding to two different jet velocities converge in the fully boiling regime. The average heat transfer coefficient in this regime is equal to h_{nb}, which is independent of jet velocity.

The bounding envelopes in Figure 5(a) show the sensitivity of the model to changes in the average single-phase Nusselt number ($\overline{\mathrm{Nu}}_{ref}$) and nucleate boiling heat transfer coefficient (h_{nb}) traversing the regimes as a function of heat flux. In the single-phase regime, an increase in $\overline{\mathrm{Nu}}_{ref}$ delays the appearance of nucleate boiling to higher heat fluxes; this is because the nucleate boiling heat transfer coefficient must exceed a higher single-phase heat transfer coefficient per the transition criteria imposed by the model. As the boiling front creeps inward toward the center of each jet unit cell in the partial boiling regime, the nucleate boiling heat transfer increasingly becomes the dominant heat transfer mechanism, reducing the impact of changes in $\overline{\mathrm{Nu}}_{ref}$ on the predictions and increasing the impact of h_{nb}. In the fully boiling regime, h_{nb} exclusively impacts the predicted superheat. These sensitivity results illustrate the critical need to select correlations appropriate for the specific system under consideration for the current modeling approach to provide accurate predictions.

The effects of changes in the other two parameters on the boiling curve predictions, namely the single-phase stagnation Nusselt number ($\mathrm{Nu}_{0,ref}$) and the single-phase width parameter (σ), are not included in Figure 5(a) for clarity, and because they have a comparatively smaller effect. The single-phase width parameter, σ, primarily affects model predictions in the partial boiling regime; the maximum deviation of predicted superheat is 4.43% (*i.e.*, deviation of 3.04 °C) for a relative change of 15% in σ from the baseline prediction (for which $\sigma = 1$) at a heat flux of 6 W/cm^2 for the jet velocity of 1 m/s. Similarly, the stagnation Nusselt number ($\mathrm{Nu}_{0,ref}$) has the greatest impact on the partial boiling regime, though the maximum deviation of predicted superheat is only 0.68% (*i.e.*, deviation of 0.49 °C) for a relative change of 15% in $\mathrm{Nu}_{0,ref}$ from the baseline prediction at a heat flux of 16 W/cm^2 for the jet velocity of 4 m/s. While the single-phase width parameter and the stagnation Nusselt number do impact model results, the model predictions are significantly more sensitive to the average single-phase Nusselt number and the nucleate pool boiling heat transfer coefficient.

5 Model validation

For validation of the proposed modeling approach, model predictions are compared with experimental results obtained in the current work as well as those available in the literature for which the geometrical and operating parameters lie within the ranges of available correlations. In addition, comparisons were limited to those studies in which the jet array covers all of a uniformly heated area. While there are a number of experimental studies on two-phase jet array impingement ([1], [10], [18], [20–30]), only Rau and Garimella [1] and de Brún *et al.* [24] meet these criteria and are used in this validation. While Rau and Garimella [1] use a thin-film heater which extends beyond the boundary of the outer jet unit cells in the arrays tested, the lack of lateral conduction in the thin-film and the use of infrared thermography to acquire spatial temperature measurements allow the heat transfer data within the array to be extracted and used for validation. The local temperature data acquired within jet unit cells is also useful for comparison with the local profile predicted by the model. In the experimental study of de Brún *et al.* [24], a 35 mm × 35 mm × 3 mm copper plate is heated from below by a large copper heater over a central 15 mm × 15 mm area. Geometric features are incorporated in the copper plate to prevent heat spreading outside of the heated area. Because the 15 mm × 15 mm heated area on the copper chip surface extends to the edge of the outer unit cells for their 3 × 3 array of 1 mm jets ($s/d = 5$), the average surface temperature data reported in Ref. [24] is useful for validation. The working fluids used in these studies are HFE-7100 [1] and distilled water [24]. For each comparison, the choice of correlations from the literature was based on their applicability to the parameter ranges of the experimental data obtained here, as well as their providing the best fit to the data, as we recommend based on the analysis performed in Section 4.

5.1 Comparison to the current experimental results

The predictions of the semi-empirical model developed here are validated against the area-averaged surface temperatures obtained as described in Section 3.4. The fluid is HFE-7100 and the inlet subcooling is 8 °C. The flow rate for all cases is 1300 ml/min, which corresponds to Reynolds numbers of 5400 for the 3×3 array and 3300 for the 5×5 array. Three different nondimensional orifice-to-target spacings, H/d, are tested using the 3×3 array, namely, 0.5, 1 and 4. Spacings of $H/d = 1$ and 4 are tested using the 5×5 array. Table 1 summarizes the geometrical parameters and operating conditions. Correlations used in this comparison include: Martin [16] for area-averaged single-phase Nusselt number, Li and Garimella [15] for the stagnation Nusselt number, and Stephan and Abdelsalam [32] for the nucleate boiling heat transfer coefficient ($C_4 = 1.7$). A summary of these correlations can be found in Table 2.

The boiling curves obtained from the experiments and predicted by the model for the 3×3 and 5×5 jet arrays are shown in Figure 6 and Figure 7, respectively, with a mean absolute error in the predicted

surface temperature of 0.53 °C compared to the experiments. For the three orifice-to-target spacings, the model predicts small differences in the curves in the single-phase and partial boiling regimes; the predicted surface temperatures are identical for all cases when boiling occurs over the entire surface, as the nucleate pool boiling heat transfer coefficient predicted by the correlation is independent of gap height. In the experimental boiling curves, small differences in boiling curve slopes are also observed during single-phase heat transfer among the three orifice-to target spacings, and the magnitude of measured superheat is in reasonable agreement with the model predictions. Discrepancies in superheat within the single-phase regime might be attributed to experimental parameters that are slightly outside the applicability range of the correlations. However, once boiling occurs on the entire surface, differences in surface superheat between the three confinement heights are much smaller than in the single-phase regime, and both the experimental boiling curves and model predictions converge. The temperature overshoot just before boiling incipience is commonly observed when a highly wetting fluid is used [19]; this phenomenon is not captured by the model.

5.2 Comparison to studies in the literature

The model predictions are first compared to local heat transfer results obtained for arrays of impinging jets by Rau and Garimella [1]. In this prior study, a thin-foil heater backed by an infrared-transparent window allowed localized temperature mapping of the heated surface during two-phase jet impingement. The fluid used was HFE-7100. Table 3 summarizes the geometrical parameters and operating conditions for the experiments in [1]. Correlations used in evaluation of the model for comparison to this data again include Martin [16] for area-averaged single-phase Nusselt number, and Li and Garimella [15] for the stagnation Nusselt number. In addition, Cooper's [33] correlation is used for the nucleate boiling heat transfer coefficient (R_p = 1 μm).

Figure 8 and Figure 9 compare model predictions with the experimental data [1] for the 3×3 and 5×5 jet arrays, respectively. The experimental data lie exclusively in either the single-phase regime or the partial boiling regime, because the experiments were terminated prior to boiling having been initiated over the entire surface. This partial boiling regime is critical to assess the model accuracy, as discussed in Section 4, because the model predictions are sensitive to the assumptions regarding the single-phase heat transfer coefficient distribution and the location of the boiling front. Excellent agreement is observed between the predicted and measured boiling curves based on the area-averaged surface temperature for all of the regimes (Figure 8(a) and Figure 9(a)), with a mean absolute error in the predicted surface temperature of 0.79 °C compared to the experimental data.

The local heat transfer coefficient distribution characteristics underpin the estimate of area-averaged surface temperature. Figure 8(b) and Figure 9(b) compare the predicted and measured local heat transfer

coefficients as a function of the radial coordinate and normalized with respect to the value at the stagnation point, for the maximum heat flux tested. The model predicts a bell-shaped distribution of the heat transfer coefficient in the single-phase region, and a uniform heat transfer coefficient in the boiling region. The experimental local heat transfer coefficient profile is obtained by averaging values along annular bands. There is reasonable agreement between the heat transfer coefficient profile assumed by the semi-empirical model and the local experimental data in the single-phase and boiling regions.

The excellent agreement of the predictions for the area-averaged surface temperature within the single-phase regime of the boiling curves (Figure 8(a) and Figure 9(a)) indicates that Martin's correlation [16] accurately estimates the single-phase area-averaged Nusselt number for this experiment. Also, from the data for the local heat transfer coefficients (Figure 8(b) and Figure 9(b)), it is apparent that the boiling heat transfer coefficient measured in Ref. [1] is well-represented by the Cooper correlation [33]. However, the stagnation heat transfer coefficient is, in general, slightly over-predicted by the correlation of Li and Garimella [15]; the discrepancies may be due to the use of the correlation outside the original ranges for which it was developed.

Area-averaged results from a recent study by de Brún *et al.* [24] are now compared against model predictions in Figure 10. The geometric configuration consists of a 3×3 array of 1 mm diameter jets, jet-to-jet spacing (*s/d*) of 5, and an orifice-to-target distance (*H/d*) of 2. The jets of distilled water impinge onto a 15 mm × 15 mm copper surface under submerged and confined conditions. The average surface temperature is extrapolated from thermocouples embedded in the copper surface. As summarized in Table 3, operating parameters include a subcooling of 8 °C and flow rates of 500 mL/min (v_j = 1.18 m/s) and 670 mL/min (v_j = 1.57 m/s). Both of the tests included in this comparison were carried through to a critical heat flux condition. To account for the lower confinement height (*H/d* = 2), the correlation of Campbell *et al.* [17] is used for the area-averaged single-phase Nusselt number. Li and Garimella [15] and Cooper [33] (R_p = 1 μm) are again used for $Nu_{0,ref}$ and h_{nb}, respectively. The trend in area-averaged single-phase performance with respect to flow rate is properly captured, indicating that the Campbell *et al.* correlation [17] accurately predicts the average single-phase Nusselt number. Partial-boiling heat transfer is represented by the model prediction with reasonable accuracy, and, as suggested by de Brún *et al.* [24], Cooper's correlation [33] predicts the fully boiling regime heat transfer coefficient well. The final jump in surface temperature (shift of the curve to the right in Figure 10) at the onset of critical heat flux is not captured by the model, which does not include a prediction of critical heat flux. Excluding these points, the mean absolute error in surface temperature prediction is 1.34 °C for this dataset.

5.3 Summary of comparisons

Figure 11 compares the predicted and measured boiling curves for de Brún *et al.* [24], Rau and Garimella [1], and the jet array configuration investigated in the current study. Apart from the outliers in the current data set due to temperature overshoot at incipience and onset of critical heat flux (denoted as open symbols in Figure 11), experimental data in all three cases, which include the single-phase, partial boiling, and fully boiling regimes, are well-predicted. The mean absolute percentage error (MAPE) in comparing the current experimental results with model predictions in terms of the difference between surface temperature and jet inlet temperature is 3.61%. In this calculation, the data points corresponding to temperature overshoot at boiling incipience were omitted. For the comparisons to Rau and Garimella [1] and de Brún *et al*. [24], the MAPE is 3.75% and 4.42%, respectively. In the MAPE calculation for de Brún *et al*. [24], the data points corresponding to critical heat flux were omitted. The overall mean absolute error across all experimental data points is 3.88%.

6 Conclusions

A semi-empirical model is presented for the prediction of area-averaged two-phase heat transfer from a surface subjected to jet array impingement. The modeling approach is based on experimental observations of single-phase and boiling heat transfer occurring simultaneously at different portions of the surface. The semi-empirical model uses available empirical correlations from the literature for single-phase jet impingement and nucleate pool boiling to predict the heat transfer coefficients in the different regions present in a representative unit cell under each jet orifice in the array.

Sensitivity of the model predictions to changes in key input variables is assessed. The analysis indicates that the predictions are most sensitive to the average single-phase Nusselt number ($\overline{\mathrm{Nu}}_{ref}$) and the nucleate boiling heat transfer coefficient (h_{nb}), while the single-phase stagnation Nusselt number ($\mathrm{Nu}_{0,ref}$) and the single-phase width parameter (σ) have more modest effects. Sensitivity of the predictions to each of these parameters is dependent on the operating regime. The model is validated with experimental data obtained in this study to demonstrate that the proposed approach properly predicts the boiling curve behavior during two-phase jet impingement across single-phase, partial boiling, and fully boiling heat transfer regimes. Comparison with experimental data available in the literature further demonstrates successful prediction of heat transfer performance. Across all experimental data comparisons considered, the mean absolute percentage error of model predictions is 3.88%. If appropriate correlations for area-averaged single-phase heat transfer, stagnation point heat transfer, and nucleate pool boiling heat transfer are chosen, the proposed model is capable of accurately predicting two-phase heat transfer from confined and submerged arrays of impinging jets. This modeling approach offers a practical

tool in the development of two-phase jet impingement cooling systems, as it allows parametric exploration of the design space.

Acknowledgements

Financial support for this work provided by members of the Cooling Technologies Research Center, a National Science Foundation Industry/University Cooperative Research Center at Purdue University is gratefully acknowledged. Carolina Mira-Hernández acknowledges financial support from the Colombia-Purdue Institute (CPI) and the Colombian department for science, technology and innovation (Colciencias). The authors thank Dr. Matthew J. Rau, who provided guidance on the modeling approach.

Appendix A. Boiling areas in square unit cell

The portion of surface area in the unit cell that experiences boiling depends on the location of the boiling front defined by Eq. 2. As shown in Figure 12, there are three possible cases for the boiling area computation according to the location where the boiling front intersects the outer edge of the unit cell:

1. When the radius of the boiling front is larger than one half of the cell diagonal, $r_{nb} > \sqrt{2}\,s/2$, boiling is not predicted to occur anywhere on the surface,

$$A_{nb} = 0 \tag{12}$$

2. When the radius of the boiling front is smaller than one half of the cell diagonal but larger than half the jet-to-jet spacing, $s/2 \le r_{nb} \le \sqrt{2}\,s/2$,

$$A_{nb} = s^2 - s\sqrt{4r_{nb}^2 - s^2} - r_b^2\left\{\pi - 4\cos^{-1}\left[s/\left(2r_{nb}\right)\right]\right\} \tag{13}$$

3. When the radius of the boiling front is smaller than half the jet-to-jet spacing, $r_{nb} < s/2$,

$$A_{nb} = s^2 - \pi r_{nb}^2 \tag{14}$$

References

[1] M. J. Rau and S. V. Garimella, "Local two-phase heat transfer from arrays of confined and submerged impinging jets," *Int. J. Heat Mass Transf.*, vol. 67, pp. 487–498, 2013.

[2] D. T. Vader, F. P. Incropera, and R. Viskanta, "Convective nucleate boiling on a heated surface cooled by an impinging, planar jet of water," *J. Heat Transf.*, vol. 114, no. 1, pp. 152–160, 1992.

[3] D. H. Wolf, F. P. Incropera, and R. Viskanta, "Local jet impingement boiling heat transfer," *Int. J. Heat Mass Transf.*, vol. 39, no. 7, pp. 1395–1406, 1996.

[4] N. M. Dukle and D. K. Hollingsworth, "Liquid crystal images of the transition from jet impingement convection to nucleate boiling Part I: Monotonic distribution of the convection coefficient," *Exp. Therm. Fluid Sci.*, vol. 12, no. 3, pp. 274–287, 1996.

[5] N. M. Dukle and D. K. Hollingsworth, "Liquid crystal images of the transition from jet impingement convection to nucleate boiling part II: Nonmonotonic distribution of the convection coefficient," *Exp. Therm. Fluid Sci.*, vol. 12, no. 3, pp. 288–297, 1996.

[6] A. M. Huber and R. Viskanta, "Effect of jet-jet spacing on convective heat transfer to confined, impinging arrays of axisymmetric air jets," *Int. J. Heat Mass Transf.*, vol. 37, no. 18, pp. 2859–2869, 1994.

[7] S. V. Garimella and R. A. Rice, "Confined and submerged liquid jet impingement heat transfer," *J. Heat Transf.*, vol. 117, no. 4, pp. 871–877, 1995.

[8] B. Weigand and S. Spring, "Multiple jet impingement - a review," *Heat Transf. Res.*, vol. 42, no. 2, pp. 101–142, 2011.

[9] D. T. Vader, F. P. Incropera, and R. Viskanta, "Local convective heat transfer from a heated surface to an impinging, planar jet of water," *Int. J. Heat Mass Transf.*, vol. 34, no. 3, pp. 611–623, 1991.

[10] C. T. Chang, G. Kojasoy, F. Landis, and S. Downing, "Confined single- and multiple-jet impingement heat transfer—II. Turbulent two-phase flow," *Int. J. Heat Mass Transf.*, vol. 38, no. 5, pp. 843–851, 1995.

[11] S. V. Garimella, "Heat transfer and flow fields in confined jet impingement," *Annu. Rev. Heat Transf.*, vol. 11, no. 11, pp. 413–494, 2000.

[12] G. K. Morris, S. V. Garimella, and J. A. Fitzgerald, "Improved predictions of the flow field in submerged and confined impinging jets using the Reynolds stress model," in *1998 6th IEEE Intersociety Conference on Thermal and Thermomechanical Phenomena in Electronic Systems (ITherm)*, 1998, pp. 362–370.

[13] C. T. Chang, G. Kojasoy, F. Landis, and S. Downing, "Confined single- and multiple-jet impingement heat transfer—I. Turbulent submerged liquid jets," *Int. J. Heat Mass Transf.*, vol. 38, no. 5, pp. 833–842, 1995.

[14] B. A. Lindeman and T. A. Shedd, "Comparison of empirical correlations and a two-equation predictive model for heat transfer to arbitrary arrays of single-phase impinging jets," *Int. J. Heat Mass Transf.*, vol. 66, pp. 772–780, 2013.

[15] C. Y. Li and S. V. Garimella, "Prandtl-number effects and generalized correlations for confined and submerged jet impingement," *Int. J. Heat Mass Transf.*, vol. 44, no. 18, pp. 3471–3480, 2001.

[16] H. Martin, "Heat and mass transfer between impinging gas jets and solid surfaces," *Adv. Heat Transf.*, vol. 13, pp. 1–60, 1977.

[17] L. A. Campbell, M. J. Ellsworth Jr, M. Iyengar, R. E. Simons, and R. C. Chu, "Experimental investigation of the heat transfer performance of arrays of round jets with

sharp-edged orifices and peripheral effluent; Convective behavior of water on a heated silicon surface," in *Proceedings of the 2005 ASME Summer Heat Transfer Conference*, 2005, pp. 17–22.
[18] R. A. Buchanan and T. A. Shedd, "Extensive Parametric Study of Heat Transfer to Arrays of Oblique Impinging Jets With Phase Change," *J. Heat Transf.*, vol. 135, no. 11, p. 111017, 2013.
[19] M. J. Rau and S. V. Garimella, "Confined jet impingement with boiling on a variety of enhanced surfaces," *J. Heat Transf.*, vol. 136, no. 10, p. 101503 1-12, 2014.
[19] 3M, 3M Novec Engineered Fluid HFE-7100 for Heat Transfer, 3M, St. Paul, MN, 2002, pp. 1-8.
[21] E. A. Browne, G. J. Michna, M. K. Jensen, and Y. Peles, "Microjet array single-phase and flow boiling heat transfer with R134a," *Int. J. Heat Mass Transf.*, vol. 53, no. 23–24, pp. 5027–5034, 2010.
[22] E. A. Browne, M. K. Jensen, and Y. Peles, "Microjet array flow boiling with R134a and the effect of dissolved nitrogen," *Int. J. Heat Mass Transf.*, vol. 55, no. 4, pp. 825–833, 2012.
[23] D. Copeland, "Single-phase and boiling cooling of a small heat source by multiple nozzle jet impingement," *Int. J. Heat Mass Transf.*, vol. 39, no. 7, pp. 1395–1406, 1998.
[24] C. de Brún, R. Jenkins, T. L. Lupton, R. Lupoi, R. Kempers, and A. J. Robinson, "Confined jet array impingement boiling," *Exp. Therm. Fluid Sci.*, vol. 86, pp. 224–234, 2017.
[25] F. J. Hong, C. Y. Zhang, W. He, P. Cheng, and G. Chen, "Confined jet array impingement boiling of subcooled aqueous ethylene glycol solution," *Int. Commun. Heat Mass Transf.*, vol. 56, pp. 165–173, 2014.
[25] S. N. Joshi, M. J. Rau, and E. M. Dede, "An experimental study of a single-device jet impingement cooler with phase change using HFE-7100 and a vapor extraction manifold," ASME International Mechanical Engineering Congress and Exposition, Proceedings (IMECE), 2013, vol. 8 B.
[27] M. Monde and Y. Mitsutake, "Critical heat flux in forced convective subcooled boiling with multiple impinging jets," *J. Heat Transf.*, vol. 117, pp. 241–243, 1996.
[27] E. N. Wang, L. Zhang, L. Jiang, J. Koo, J. G. Maveety, E. A. Sanchez, K. E. Goodson, T. W. Kenny, "Micromachined jets for liquid impingement cooling of VLSI chips," J. Microelectromechanical Syst., vol. 13, no. 5, pp. 833–842, 2004.
[28] B. Werneke, "Microjet array impingement heat transfer crossflow effects in single-phase and flow boiling," Ph.D. dissertation, Dept. Mech. Eng., Rensselaer Polytechnic Inst., Troy, NY, 2015.
[30] S. Wu, C. H. Shin, K. M. Kim, and H. H. Cho, "Single-phase convection and boiling heat transfer: Confined single and array-circular impinging jets," *Int. J. Multiph. Flow*, vol. 33, no. 12, pp. 1271–1283, 2007.
[31] M. T. Meyer, I. Mudawar, C. E. Boyack, and C. A. Hale, "Single-phase and two-phase cooling with an array of rectangular jets," *Int. J. Heat Mass Transf.*, vol. 49, no. 1–2, pp. 17–29, 2006.
[32] K. Stephan and M. Abdelsalam, "Heat-transfer correlations for natural convection boiling," *Int. J. Heat Mass Transf.*, vol. 23, no. 1, pp. 73–87, 1980.
[33] M. G. Cooper, "Heat flow rates in saturated nucleate pool boiling-A wide-ranging examination using reduced properties," *Adv. Heat Transf.*, vol. 16, pp. 157–239, 1984.

List of Tables

List of Figures

Figure 11. Comparison of predicted boiling curves against experimental results from de Brún et al. [23], Rau and Garimella [1], and the current experiments. Empty symbols for the current data set correspond to overshoot at boiling incipience and those for de Brún et al. [23] correspond to critical heat flux.

Figure 12. Cases for boiling area computation in a square unit cell.

Table 1. Geometrical parameters and operating conditions for the two-phase jet array impingement experiments performed in the current study.

N	d (mm)	H/d	s/d	$\dot{V}$ (ml/min)	v_j (m/s)	Re	ΔT_{sub} (°C)	p_{op} (kPa)	Pr
3×3	2	4 1 0.5	3.33	1300	0.77	5450	8	101.3	7.85
5×5	1.2	4 1	3.33	1300	0.77	3300	8	101.3	7.85

Table 2. Empirical correlations used in model validation with current experimental data set.

Correlation	Ref
Area-averaged single-phase Nusselt number $\overline{\mathrm{Nu}}_{ref} = 0.5\,\mathrm{Re}^{0.667}\,\mathrm{Pr}^{0.42}\times\left\{1+\left(\frac{(H/d)\sqrt{\pi}/2}{0.6(s/d)}\right)^{6}\right\}^{-0.05}$ $\times\left(\frac{\sqrt{\pi}}{s/d}\right)\frac{1-1.1\sqrt{\pi}/(s/d)}{1+0.1(H/d-6)\sqrt{\pi}/(s/d)}$ $2000 \le \mathrm{Re} \le 100{,}000$ $4.43 \le s/d \le 14.01$ $2 \le H/d \le 12$	Martin [16]
Stagnation Nusselt number $\mathrm{Nu}_{0,ref} = 1.409\,\mathrm{Re}^{0.497}\,\mathrm{Pr}^{0.444}\left(l/d\right)^{-0.058}\left(2r_{eq}/d\right)^{-0.272}$ $4000 \le \mathrm{Re} \le 23000$ $1.59\ \mathrm{mm} \le d \le 6.35\ \mathrm{mm}$ $1 \le H/d \le 5.0$ $0.25 \le l/d \le 12$ $r_{eq} = 5.64$ $7.1 \le \mathrm{Pr} \le 25.2$	Li and Garimella [15]
Nucleate pool boiling heat transfer coefficient $h_{nb} = C_4 q''^{0.745}$ $3\times10^{-3} \le p_{op}/p_c \le 0.78$ Fluid: Refrigerants	Stephan and Abdelsalam [32]

Table 3. Geometrical parameters and nominal operating conditions for jet array experiments available in the literature for comparison.

N	d (mm)	H/d	s/d	$\dot{V}$ (ml/min)	v_j (m/s)	p_{op} (kPa)	ΔT_{sub} (°C)	Re_j	Fluid	Ref
3×3	1.25	4	4	450 900 1800	0.68 1.35 2.72	120	10	3144 6289 12577	HFE-7100	Rau and Garimella [1]
5×5	0.75	4	4	450 900 1800	0.68 1.35 2.72	120	10	1887 3773 7546	HFE-7100	Rau and Garimella [1]
3×3	1	2	5	500 670	1.18 1.57	100	8	3685 4903	Water	de Brún *et al*. [24]

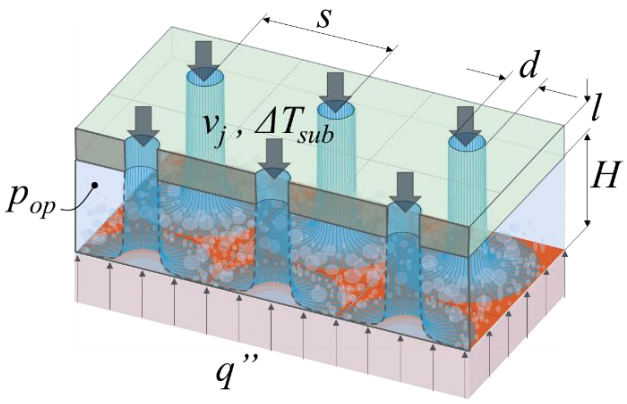

Figure 1. Geometrical parameters and operating conditions relevant in jet array impingement heat transfer.

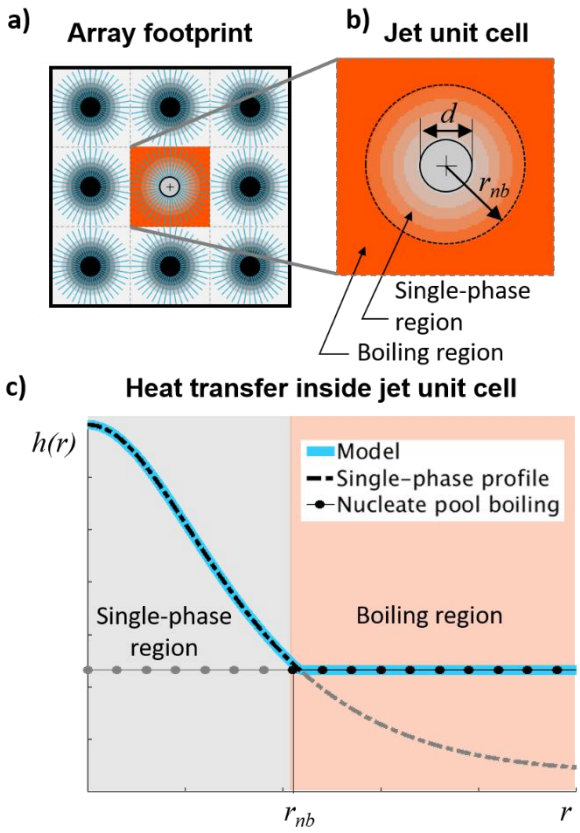

Figure 2. Modeling approach for (a) heat transfer in a jet array based on the analysis of (b) a jet unit cell, inside which single-phase and boiling regions are defined based on (c) expected distributions of the heat transfer coefficient.

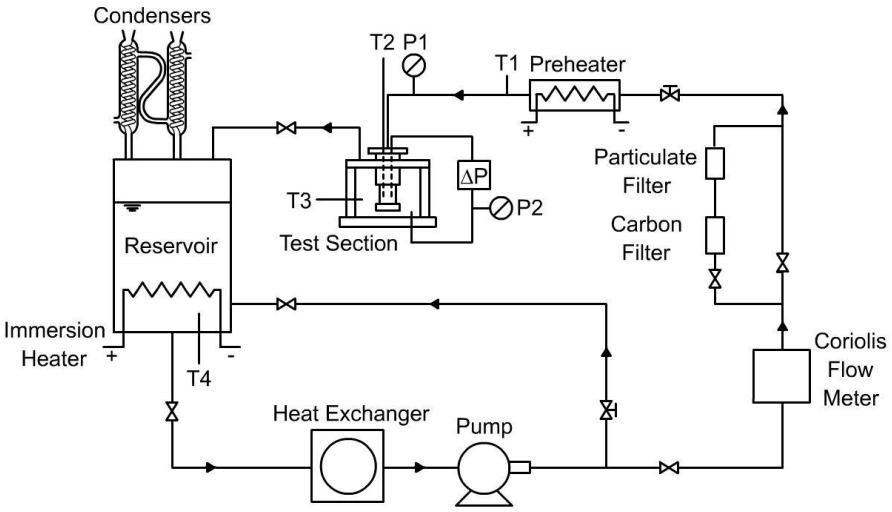

Figure 3. Flow loop schematic diagram.

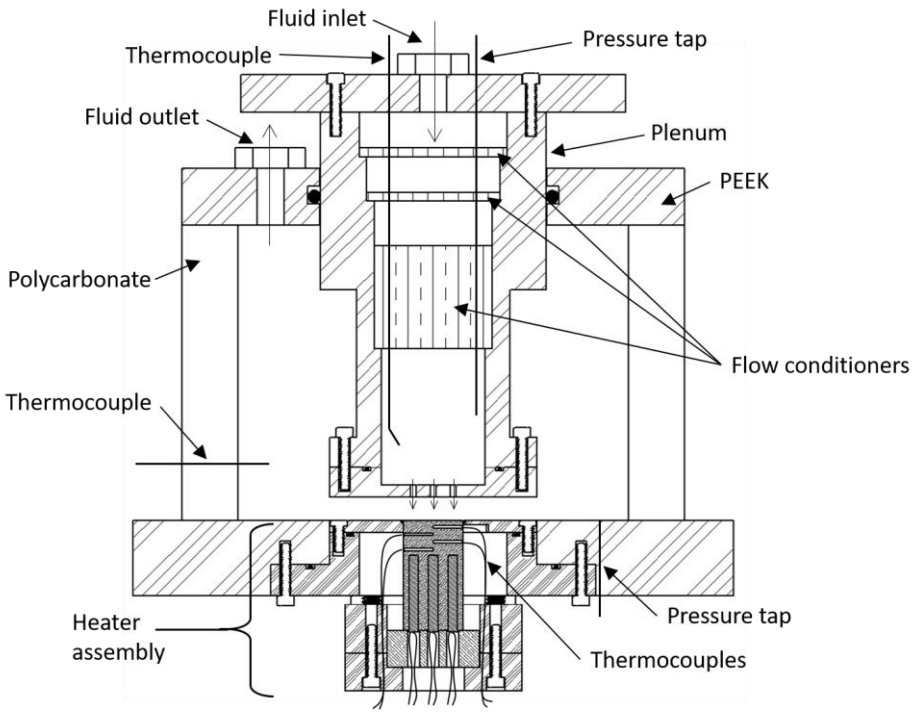

Figure 4. Cross-sectional view of test section.

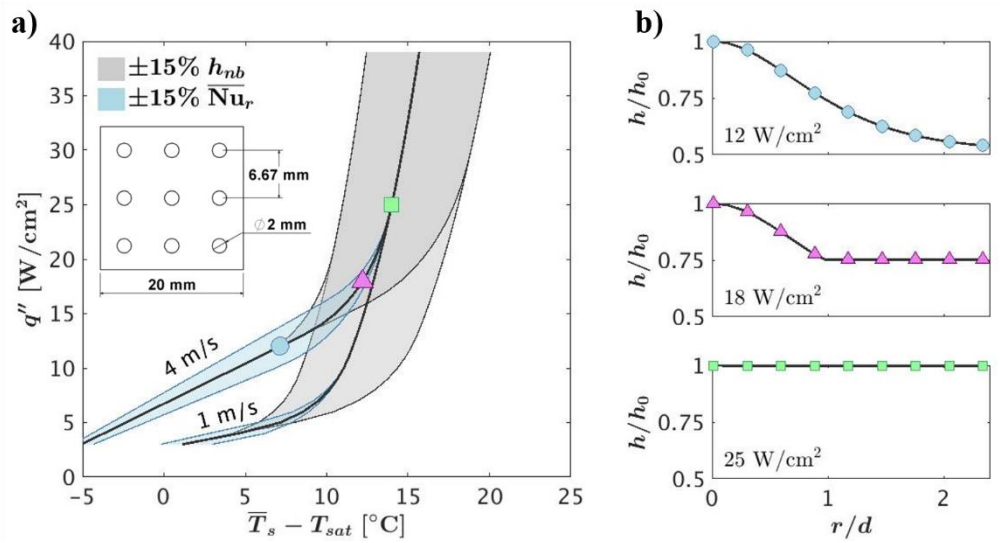

Figure 5. Sensitivity analysis results: (a) blue and gray shaded envelopes correspond to changes in superheat predictions for a ±15% variations in area-averaged single-phase Nusselt number and nucleate pool boiling heat transfer coefficient, respectively; (b) predicted radial heat transfer coefficient distributions for a single unit cell at three different heat fluxes at a jet velocity of 4 m/s, corresponding to the symbols shown in (a). Correlations used for the baseline prediction: $\overline{\mathrm{Nu}}_{ref}$ [16], $\mathrm{Nu}_{0,ref}$ [15], h_{nb} [32].

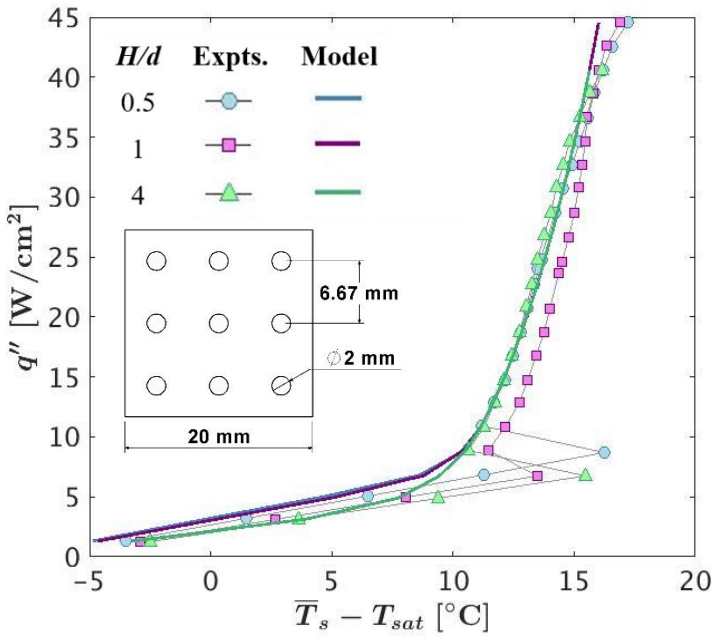

Figure 6. Model predictions of area-averaged surface superheat for the conditions of Table 1 for the 3×3 array at a flow rate of 1300 mL/min (v_j = 0.77 m/s) compared to the current experimental data. Correlations used in this comparison: $\overline{\mathrm{Nu}}_{ref}$ [16], $\mathrm{Nu}_{0,ref}$ [15], h_{nb} [32].

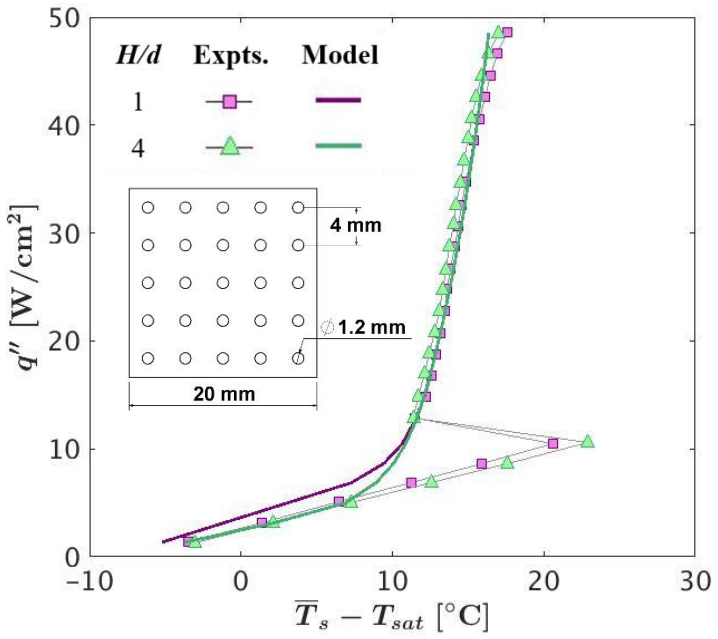

Figure 7. Model predictions of area-averaged surface superheat for the conditions of Table 1 for the 5×5 array at a flow rate of 1300 mL/min (v_j = 0.77 m/s) compared to the current experimental data. Correlations used in this comparison: $\overline{\mathrm{Nu}}_{ref}$ [16], $\mathrm{Nu}_{0,ref}$ [15], h_{nb} [32].

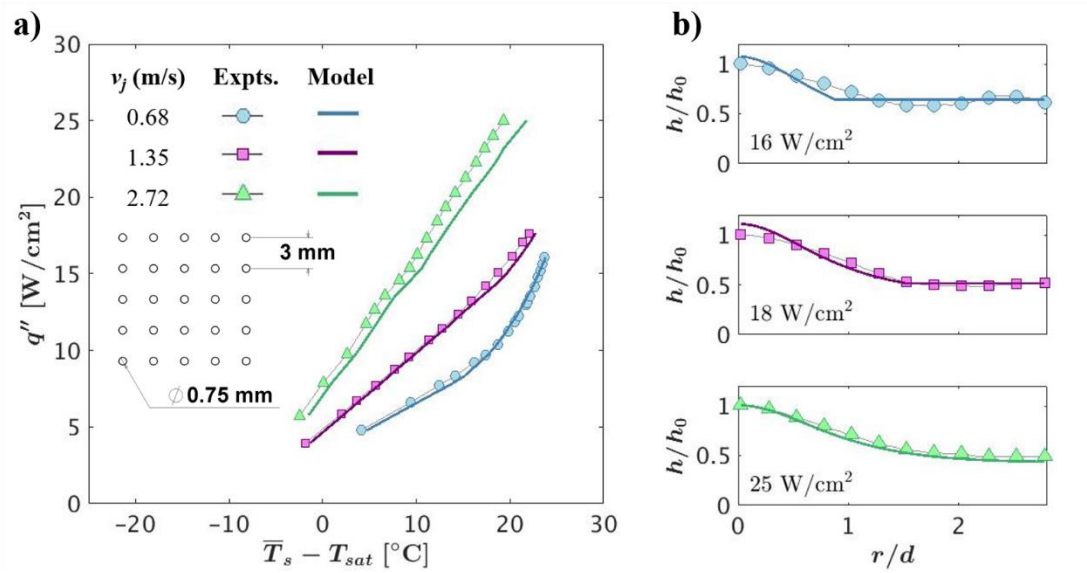

Figure 8. Model predictions for the conditions of Table 3 for the 3×3 array compared to the experimental data in [1]: (a) Boiling curves based on the area-averaged surface superheat, and (b) local heat transfer coefficient distributions in the central jet unit cell for the maximum heat flux tested at each jet velocity. Model predictions are shown as solid lines colored to distinguish between the different labelled flow rates. Correlations used in this comparison: $\overline{\mathrm{Nu}}_{ref}$ [16], $\mathrm{Nu}_{0,ref}$ [15], h_{nb} [33].

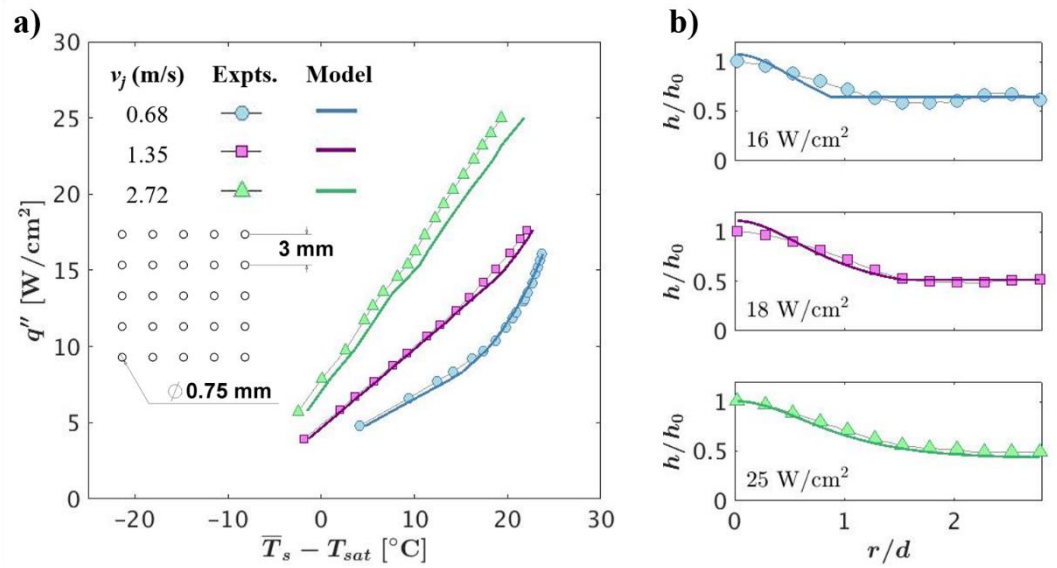

Figure 9. Model predictions for the conditions of Table 3 for the 5×5 array compared to the experimental data in [1]: (a) Boiling curves based on area-averaged surface superheat, and (b) local heat transfer coefficient distributions in the central jet unit cell for the maximum heat flux tested at each jet velocity. Model predictions are shown as solid lines colored to distinguish between the different labelled flow rates. Correlations used in this comparison: $\overline{\mathrm{Nu}}_{ref}$ [16], $\mathrm{Nu}_{0,ref}$ [15], h_{nb} [33].

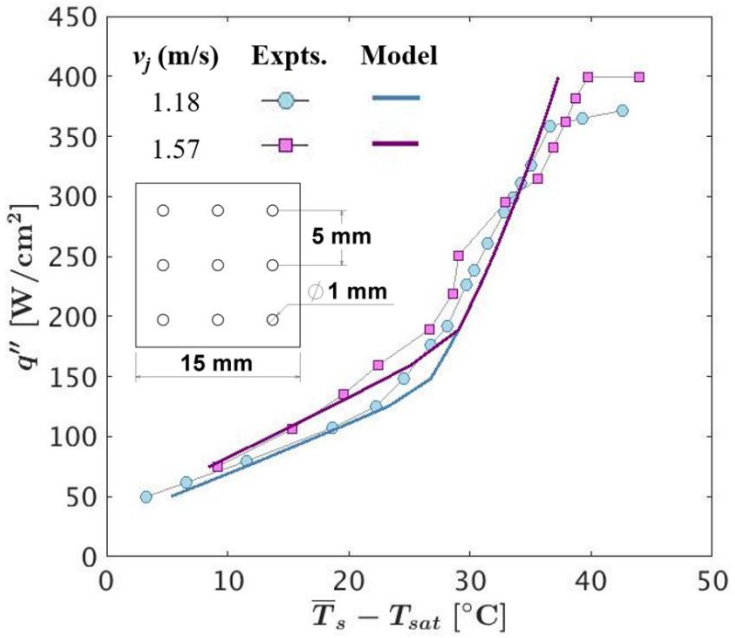

Figure 10. Comparison of boiling curves predicted by the model against the experimental data of de Brún *et al.* [23] for a 3×3 array and flow rates of 500 mL/min (v_j = 1.18 m/s) and 670 mL/min (v_j = 1.57 m/s). Correlations used in this comparison: $\overline{\mathrm{Nu}}_{ref}$ [17], $\mathrm{Nu}_{0,ref}$ [15], h_{nb} [33].

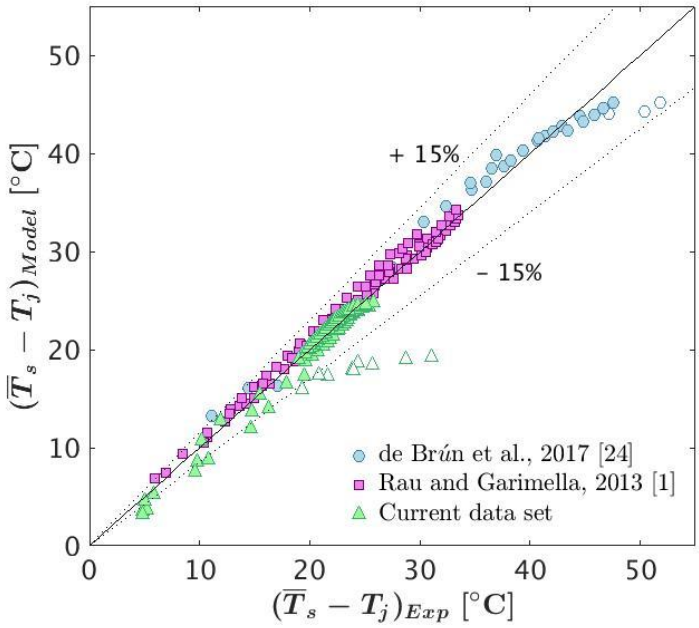

Figure 11. Comparison of predicted area-averaged surface superheat against experimental results from de Brún *et al.* [24], Rau and Garimella [1], and the current experiments. Empty symbols for the current data set correspond to overshoot at boiling incipience and those for de Brún *et al.* [24] correspond to critical heat flux.

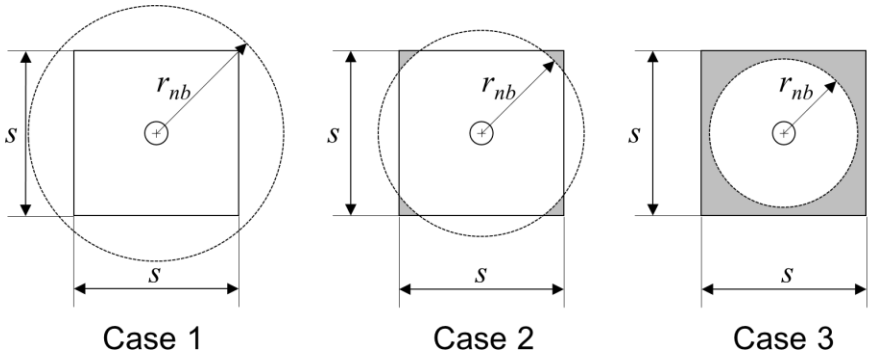

Figure 12. Cases for boiling area computation in a square unit cell.